Journal of Zhejiang University-SCIENCE A (Applied Physics & Engineering)
ISSN 1673-565X (Print); ISSN 1862-1775 (Online)
www.jzus.zju.edu.cn; www.springerlink.com
E-mail: jzus@zju.edu.cn

A novel stress-based formulation of finite element analysis[#]

Himanshu GAUR[†1,2], Lema DAKSSA[2], Mahmoud DAWOOD[2], Nitin Kumar SAMAIYA[3]

[1]*Institute of Structural Mechanics, Bauhaus–Universität Weimar, Marienstrasse 15, D-99423 Weimar, Germany*

[2]*Department of Civil Engineering, Middle East College, Knowledge Oasis Muscat (KOM), Al Rusayl, Muscat 124, Oman*

[3]*Department of Civil Engineering, Jaypee University of Engineering and Technology, Guna (M.P.)-473226, India*

[†]E-mail: himanshugaur82@gmail.com

Received Sept. 6, 2020; Revision accepted Nov. 29, 2020; Crosschecked May 18, 2021

Abstract: This paper demonstrates a novel formulation of structural analysis. A novel stress-based formulation of structural analysis for material nonlinear problems was proposed in earlier work. In this paper, this methodology is further extended for 3D finite element analysis. The approach avoids use of elastic moduli as the material input in the analysis procedure. It utilizes the whole stress-strain curve of the material. It can be shown that this analysis procedure solved the nonlinear or plasticity problem with relative ease. This paper solves a uniaxial bar, in which the results are compared with the solutions of Green-Lagrange strain and Piola-Kirchhoff stresses. The uniaxial bar is also solved by a regression model in the 'scikit-learn' module in Python. The second problem solved is of a beam in pure bending for which the energy release rate is measured. For the beam in pure bending, the bending moment carrying capacity of the beam section is evaluated by this methodology as the crack propagates through the depth of the beam. It can be shown that the methodology is very simple, accurate, and clear in its physical steps.

Key words: Computational methods; Machine learning; Regression method; Material non-linear analysis; Finite element analysis
https://doi.org/10.1631/jzus.A2000397 **CLC number:** TU39

1 Introduction

The objective of the computational methods is to be able to best simulate the structural response when subjected to loading. It should be able to match the response of the structural body with the experimental behavior. These computational procedures simplify the analysis. It is not possible to perform laboratory test for all structural components that are used for engineering applications. Thus, the simplified approaches are adopted. For example, the stress-strain diagram is tested for the longitudinal sample subjected to axial load only, but the same stress-strain behavior is also used in the analyses of beam bending, plates, a 3D body, and torsion.

In this paper, the stress-based approach is further extended to a 3D formulation (Gaur, 2019; Gaur and Srivastav, 2020). Current, the state-of-the-art finite element analysis uses Green-Lagrange strain and its energy conjugate Piola-Kirchhoff stress. These energy conjugates are also used in the analysis when the response of the structural body is desired for large deformations. With the basic derivation of the Green-Lagrange strain, it is possible to successfully avoid rigid body rotation of the element, but higher order terms that appear in the Green-Lagrange strain expression lack the physical insight of the formulation, and therefore, the same is true with the basic derivation of Piola-Kirchhoff stress (Rabczuk et al., 2019; Bathe, 2014). In this paper, we set out to measure the accuracy of these energy conjugates. In our assumption, the most accurate values of stresses and strains

[#] Electronic supplementary materials: The online version of this article (https://doi.org/10.1631/jzus.A2000397) contains supplementary materials, which are available to authorized users

ORCID: Himanshu GAUR, https://orcid.org/0000-0001-9299-8506; Lema DAKSSA, https://orcid.org/0000-0001-5382-6621; Mahmoud DAWOOD, https://orcid.org/0000-0001-9084-8811; Nitin Kumar SAMAIYA, https://orcid.org/0000-0001-8294-6462

are true stress and true strains as these accommodate the effects of area change during large deformation and are obtained from real experimental results of material. It is evident that, of interest is the response of the structure when it undergoes large deformations (Rabczuk and Belytschko, 2007; Areias and Rabczuk, 2013; Areias et al., 2014; Budarapu et al., 2014b).

The relation of shear stress function is also derived from the normal stress function. A comparison is made with the existing results in the linear range which shows good and accurate agreement. The derivation is made in much the same way as the modulus of rigidity can be derived from the modules of elasticity in the classical theory (Timoshenko and Goodier, 1970).

Modeling crack growth with finite element analysis has always been of interest (Rabczuk et al., 2007, 2010a; Chau-Dinh et al., 2012; Talebi et al., 2015; Areias et al., 2018). One of the pioneering works on crack propagation for concrete structures in which crack propagation was modeled with finite element analysis is by Hillerborg et al. (1976). In fracture mechanics, crack propagation was also modeled with plasticity analysis by phase-field modeling (Amiri et al., 2014a; Areias et al., 2016; Areias and Rabczuk, 2017). Hillerborg et al. (1976) proposed a mathematical model which utilized the 'energy release rate' parameter in order to model crack propagation in the beam. In their formulation, they used the experimental results of stress-stain data from concrete samples which were recorded by Evans and Marathe (1968). In the experiment of Evans and Marathe (1968), the readings of the stress-strain curve, especially the falling part of the stress-strain curve after the peak, were taken at a controlled deformation in order to capture the behavior of concrete and to avoid the sudden rupture of the brittle material (Rabczuk and Belytschko, 2004; Rabczuk et al., 2008, 2010b; Areias et al., 2013; Budarapu et al., 2014a; Talebi et al., 2014). In this paper, we solve the same problem. For a beam in pure bending, the energy release rate is evaluated and the bending moment carrying capacity of the beam section is evaluated as the crack propagates through the depth of the section by the proposed methodology. The energy release rate is evaluated by the Griffith theory (Griffith, 1921).

The proposed methodology can be regarded as a stress-based analysis procedure as it is necessary to know the stress distribution inside the structural body through proper modeling assumptions. It is not identical to the displacement-based approach adopted so far for structural analysis (Talebi et al., 2014; Zhang et al., 2020). This methodology avoids the use of any elastic moduli in the analysis procedure; instead, stress and strain functions are used.

With the formulations of Hillerborg et al. (1976), and the experimental data that was utilized in the analysis, it can be said that once the material fiber is loaded, it undergoes three different phases that are studied in the literature—linear behavior, nonlinear range, and finally it undergoes fracture if the load is increased beyond capacity. These three different phases are studied differently, according to the requirements at different periods in the literature (Amiri et al., 2014b; Ghorashi et al., 2015; Vu-Bac et al., 2018; Guo et al., 2019). The proposed formulation solves the structural problem for all these three phases together. It will be seen that the proposed formulation gives largely more accurate results than the classical linear or displacement-based approaches.

The proposed approach can be used not only for design purposes but also for analysis where a large deformation of the structures is of interest. For example, the stress-strain curve of the material can be used until the attainment of maximum stress if the analysis is required for design purposes. The stress-strain curve can be used up to the fracture point if the response of the structure is required for large deformations. We have used the stress-strain curve up to the fracture point as we intend to observe the structural behavior for large deformations.

Machine learning uses a set of already available data, uses suitable algorithms, and makes predictions. The process tends to, in some ways, let machines learn from past data. It is much like how humans learn from previous experiences. The concept was first used by Warren S. McCulloch, a neuroscientist, and Walter Pitts, a logician in 1943 (McCulloch and Pitts, 1990). In the last few decades, machine learning has gained much research interest because of its vast applications in different fields, such as image and voice recognition or banking, and in many other commercial applications. Recently, its applications have also been developed in computational mechanics, where the approximate solutions of partial differential equations are found via machine learning (Lagaris et al., 1998; Berg and Nyström, 2018; Raissi

and Karniadakis, 2018; Sirignano and Spiliopoulos, 2018; Weinan and Yu, 2018; Anitescu et al., 2019; Guo et al., 2019; Samaniego et al., 2020).

In this paper, we have used raw data on stress and strain of mild steel as the direct inputs in generating a regression model in machine learning. With a suitable regression model and curve fitting, material nonlinear analysis was performed for solving structural problems. A Python tool is used in making the machine learning model in nonlinear regression in order to gain the best fit of the stress-strain data (van Rossum and Drake, 2009). Other tools, such as Matlab or Excel can also be used for this purpose.

2 Methodology–basic formulation

As explained previously, our methodology utilizes the whole stress-strain curve in the form of stress function and strain function as the material input in the analysis procedure (Gaur, 2019; Gaur and Srivastav, 2020). True stress and true strain are used rather than engineering stress and engineering strain in order to accommodate the effect of large deformations. In this paper, the basic derivation of finite element analysis is proposed. It is emphasized that Gauss's divergence theorem is applicable not only in the linear range of the loading condition but also in the nonlinear range or plastic range of the material behavior as it is just the force balance equation (Gauss, 1867).

2.1 Material input—true stress and true strain functions

In this study, the stress-strain graph of mild steel was used which was obtained from a tension test in the laboratory on mild steel (ES6, 2018). The stress and strain components were first converted to true stress and true strains. The values were mapped in the reference coordinate system (r) from −1 to +1, very much as the natural coordinate system of finite element analysis (Bathe, 2014). From the raw data of true stress and true strain, the following true stress and true strain functions were derived by the nonlinear regression method in Python:

$$\sigma(r)=473.9\mathrm{e}^{0.06458r}-\frac{0.03438}{\mathrm{e}^{9.5r}}, \tag{1}$$

$$\varepsilon(r)=0.01545r+0.01546. \tag{2}$$

The variations of these true stress and true strain functions in reference coordinate system (r) can be observed in the following Figs. 1 and 2 drawn in Matplotlib.

It is interesting to note that the whole stress-strain graph of material (Fig. 1) is utilized in the analysis up to the fracture point as we intended to observe the structural behavior for large deformations.

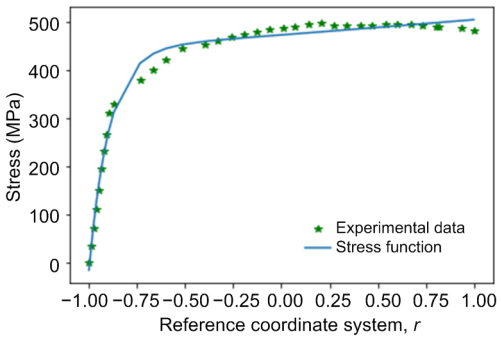

Fig. 1 Variation of the true stress function along with experimental data in the reference coordinate system

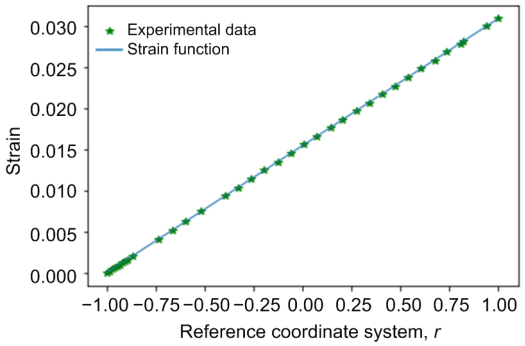

Fig. 2 Variation of the true strain function along with experimental data in the reference coordinate system

2.2 Deformation function

The strain function expressed in Eq. (2) can be written as $\varepsilon=\mathrm{d}u/\mathrm{d}r=0.01545r+0.01546$ or, $\mathrm{d}u=(0.01545r+0.01545)\mathrm{d}r$, taking the integration of both sides, $u=\int(0.01545r+0.01545)\mathrm{d}r$, integrating, $u=0.00773r^2+0.01546r+c$. At $r=-1$, $u=0$, hence, $0=0.00773(-1)^2+0.01545(-1)+c$, solving, $c=0.00773$, hence,

$$u=0.00773r^2+0.01546r+0.00773. \tag{3}$$

2.3 Proposed finite element formulation

Throughout the text the Einstein summation convention (Einstein, 1916) is used in this paper. Fig. 3 shows a typical 3D body in Cartesian coordinate system, where the normal stress σ_{ij} and shear stress τ_{ij} components are shown.

In the finite element derivation, we wish to emphasize that in the 3D continuum of a structural body, either it is linear or a linear range of the loading condition, the divergence theorem is satisfied at each point of the loading condition (Gauss, 1867). Detailed derivation of finite element formulation can be glanced in the electronic supplementary material.

Hence, the force balance equation that is used abundantly in the analysis can be written as

$$473.9\mathrm{e}^{0.06458r}-\frac{0.03438}{\mathrm{e}^{9.5r}}=\frac{F_x}{A}, \tag{4}$$

where A is the total area of the element cross section in the YZ-plane, and F_x is the force acting in x-direction on the element (Fig. 3b). Eq. (4) is used to find the reference coordinate system (r) for the structural body subjected to loading.

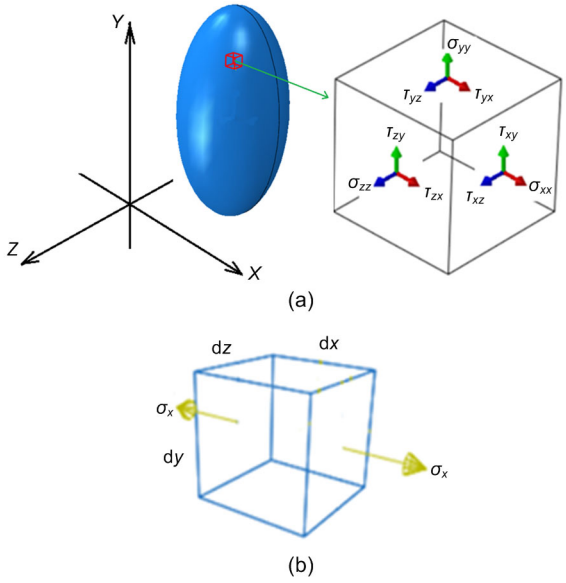

Fig. 3 3D coordinate system

(a) Stress components in a 3D body; (b) A 3D element subjected to uniaxial stress

2.4 Derivation of shear stress and shear strain functions from normal stress and normal strain functions

In this section, the shear stress and shear strain functions are derived from the normal stress and normal strain functions. This derivation is similar to the derivation of modulus of rigidity from the modulus of elasticity in linear theory. The objective is to demonstrate that this transformation also works for large plastic deformation.

The following shear stress τ_{ij} and shear strain γ_{ij} functions are derived from the normal stress and normal strain component. Detailed derivations can be glance in the electronic supplementary material.

$$\tau_{xy}=\tau_{xz}=\tau_{yz}=473.9\mathrm{e}^{0.06458r}-\frac{0.03438}{\mathrm{e}^{9.5r}}, \tag{5}$$

$$\gamma_{xy}=\gamma_{xz}=\gamma_{yz}=2(1+\nu)(0.01545r+0.01546), \tag{6}$$

where v is Poisson's ratio of the material.

From this shear stress and shear strain functions, the average modulus of rigidity (S) (in the linear range) is evaluated as 70398.08 MPa, which is a reasonable value for mild steel of modulus of elasticity (E) value 184128.9683 MPa and can be confirmed as follows:

$$S=\frac{E}{2(1+\nu)}=\frac{184128.9683}{2(1+0.3)}=70818.83\ \text{MPa}.$$

Alternatively, these shear stress and shear strain functions can be derived from the experimental data if the sample specimen of the same material composition is tested with torsional load (Gaur and Srivastav, 2020).

3 Numerical problems

In this section, two problems are solved based on the proposed methodology. The first problem solved is of a uniaxial bar loaded axially. In this uniaxial bar, the stress and strain generated because of the axial load are compared with Green strain and with Second Piola-Kirchhoff stress. The second benchmark

problem solved is of a beam in pure bending. This problem was first solved by Hillerborg et al. (1976). For the beam in pure bending, the energy release rate is evaluated and the maximum bending moment carrying capacity of the section is determined. Of considerable note is the ease and simplicity of the analysis procedure using the proposed methodology.

3.1 Nonlinear analysis of a bar in uniaxial tension

As shown in Fig. 4, the bar deforms axially by u because of the axial load of magnitude F, A is the sectional area of the bar, and L is the initial length.

For this uniaxial case, the engineering strain is

$$\varepsilon_{\text{Engg}} = \frac{\partial u}{\partial X}. \tag{7}$$

For this uniaxial case, the Green strain can be evaluated as (Bathe, 2014)

$$E_{xx} = \frac{\partial u}{\partial X} + \frac{1}{2}\left(\frac{\partial u}{\partial X}\right)^2. \tag{8}$$

Consider that the length L of the bar is 1 m, the area of cross section A is 0.5 m^2, and the bar is loaded with force 200 MPa at the free end. In any particular section, the magnitude of stress generated can be evaluated by

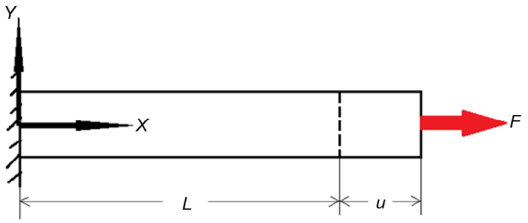

Fig. 4 A bar with uniaxial loading

$$473.9\mathrm{e}^{0.06458r} - \frac{0.03438}{\mathrm{e}^{9.5r}} = \frac{200}{0.5} = 400,$$

solving r=−0.768 546 1.

Once the value of r of the reference coordinate is evaluated, the strain can be evaluated by the strain function of Eq. (2) as, ε=0.01545(−0.768 5461)+0.015 46, solving ε=0.003 57.

This is in fact the value of the true strain. Hence, the engineering strains can be found by

$$\varepsilon_{\text{T}} = \ln\left(1+\varepsilon_{\text{Engg}}\right), \tag{9}$$

substituting the values of the true strain, 0.0035= ln(1+$\varepsilon_{\text{Engg}}$), solving $\varepsilon_{\text{Engg}}$=0.00357.

From the engineering strain ($\varepsilon_{\text{Engg}}$), the deformation in the bar can be evaluated by

$$\varepsilon_{\text{Engg}} = \frac{u}{L}, \tag{10}$$

rearranging and solving, u=$\varepsilon_{\text{Engg}}$, L=0.00357×1= 0.00357 m.

For this uniaxial case, the Second Piola-Kirchhoff stress can be evaluated as (Bathe, 2014)

$$\sigma^{\text{PK2}} = \frac{\sigma_{\text{Engg}}}{1+\varepsilon_{\text{Engg}}}. \tag{11}$$

The whole analysis is repeated for different loading conditions and the results are summarized in Table 1.

These tabulated results of different stresses and strains can be visualized and compared with the help of Figs. 5 and 6.

Table 1 Results of the analysis of a bar with uniaxial loading

Load, F (MN)	Reference coordinate, r	Stress by stress function (MPa)	Engineering stress (MPa)	Second Piola-Kirchhoff stress (MPa)	Deformation (m)	Engineering strain	Strain by strain function	Green strain
0	0	0	0	0	0	0	0	0
100	−0.934 30	200	199.798	199.5966	0.001 01	0.001 01	0.001 01	0.001 01
150	−0.880 60	300	299.449	298.8990	0.001 84	0.001 84	0.001 84	0.001 84
200	−0.768 50	400	398.577	397.1592	0.003 57	0.003 57	0.003 57	0.003 58
245	0.517 34	490	478.647	467.5561	0.023 72	0.023 72	0.023 45	0.024 00
250	0.830 16	500	485.928	472.3751	0.028 69	0.028 69	0.028 29	0.029 10

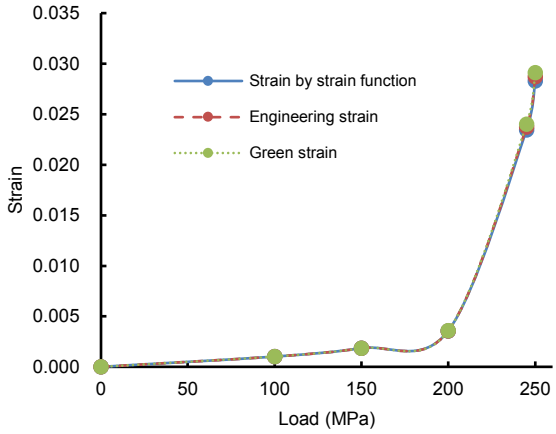

Fig. 5 Comparison of different strain components for a bar with uniaxial loading

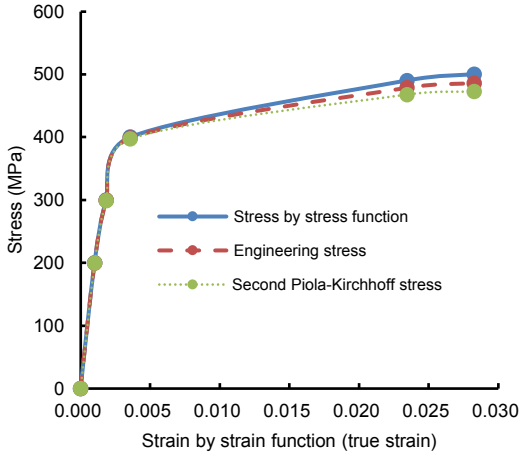

Fig. 6 Comparison of different stress components for a bar with uniaxial loading

This uniaxial bar was also solved by the machine learning regression model by the 'scikit-learn' module in Python. For the uniaxial bar problem, the sectional area and length axial load were set as independent parameters, and the deformation was set as a dependent parameter. In the machine learning model, random data of 57 inputs of a solution of the uniaxial bar, as solved in the previous section, were generated. In the neural network, two hidden layers of 120 neurons were built with the activation function 'tanh' and 'lbfgs' solvers (Pedregosa et al., 2011). With a maximum of 10000 iterations set, convergence was achieved with mean absolute error and R^2 value as 0.002281 and 0.99, respectively, for 80% of the training data whereas these are 0.7127 and 0.965 for 20% of the test data.

After training the neural network, the bar of sectional area of 0.5 m^2 and length of 1 m, which was loaded with different magnitudes of loads, was solved. The solution by the machine learning regression model is compared with that by the proposed methodology in Table 2 and the variation of results can be visualized in Fig. 7.

Table 2 Summary of results of a uniaxial bar loaded axially

Load, F (MPa)	Area (m^2)	Length (m)	Deformation (m)	
			Proposed method	Machine learning model
0	0.5	1	0	0
100	0.5	1	0.001 01	0.000 841
150	0.5	1	0.001 84	0.000 841
200	0.5	1	0.003 57	0.000 855
245	0.5	1	0.023 72	0.000 855
250	0.5	1	0.028 69	0.000 855

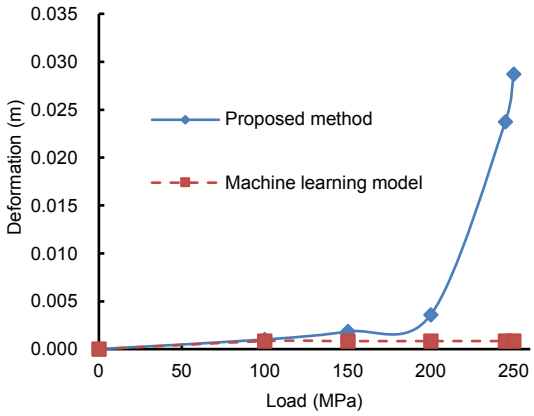

Fig. 7 Comparison of bar deformation using the proposed method and machine learning regression model

From Table 1 and Figs. 5 and 6, it can be observed that in the linear range, all the components of stresses and strains have almost similar magnitudes without any appreciable differences. In the plastic range, Green strain has higher values in the fourth digit in comparison with others.

In the plastic range, stresses by the stress function, which are in fact true stresses, have higher values than the engineering stress, which was expected that true stresses accommodate the effect of area change, and hence make physical sense. Observing the magnitude of the second Piola-Kirchhoff stress in

plastic range, its magnitude is even less than the magnitudes of engineering stresses with a difference of 15 MPa.

The results from the machine learning from Fig. 7 indicate that even the neural network regression model does not capture the nonlinear material behavior.

3.2 Crack propagation problem—a beam in pure bending

In this section, a crack propagation problem is solved. The same problem was solved by Hillerborg et al. (1976). A steel beam is subjected to pure bending as shown in Fig. 8, where b is the width of the steel beam, h is the depth of the crack and H is the total depth of the beam. So far, in fracture mechanics, the yield point was considered as fracture criteria (Griffith, 1921; Kumar, 2014). In our analysis, we consider it the same. For metals, fracture criteria could be considered at the peak stress of the stress-strain diagram.

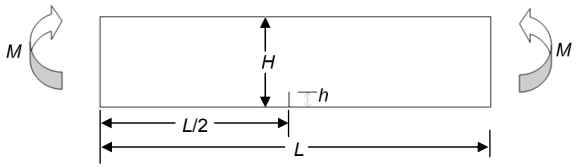

Fig. 8 A steel beam subjected to pure bending moment M

If the beam is subjected to bending, the maximum stress generated at the outer layer of the beam can be evaluated by (Gaur and Srivastav, 2020):

$$473.9\mathrm{e}^{0.06458r}-\frac{0.03438}{\mathrm{e}^{9.5r}}=\frac{4M_x}{bH^2}, \tag{12}$$

where M_x is the moment at any particular section of the beam.

The interested reader is advised to refer to article (Gaur and Srivastav, 2020) for the complete analysis of beam bending by the proposed methodology. For this beam in pure bending, the bending energy (U) stored can be evaluated by (Gaur and Srivastav, 2020)

$$U=bLH\int_{-1}^{r}\sigma\varepsilon\mathrm{d}r. \tag{13}$$

Substitute the values of the stress and strain functions from Eqs. (1) and (2), then

$$U=bLH\times\int_{-1}^{r}\left(473.9\mathrm{e}^{0.06458r}-\frac{0.03438}{\mathrm{e}^{9.5r}}\right)\left(0.01545r+0.01546\right)\mathrm{d}r. \tag{14}$$

This expression can be used to evaluate strain energy that can be stored in the beam for the given loading. If the crack propagates because of the application of loads, the energy release rate (G) can be evaluated as

$$G=\frac{\mathrm{d}U}{\mathrm{d}A}. \tag{15}$$

Substitute the expression of strain energy stored in the beam from Eq. (14), then

$$\begin{aligned}G=\frac{\mathrm{d}U}{\mathrm{d}A}&=\frac{\mathrm{d}}{\mathrm{d}A}\left[bLH\int_{-1}^{r}\left(473.9\mathrm{e}^{0.06458r}-\frac{0.03438}{\mathrm{e}^{9.5r}}\right)\right.\\&\left.\times\left(0.01545r+0.01546\right)\mathrm{d}r\right]\\&=L\int_{-1}^{r}\left[\left(473.9\mathrm{e}^{0.06458r}-\frac{0.03438}{\mathrm{e}^{9.5r}}\right)\right.\\&\left.\times\left(0.01545r+0.01546\right)\mathrm{d}r\right].\end{aligned} \tag{16}$$

Consider that a steel beam's width b=10 mm, the depth H=200 mm, and the length L=1 m. Eqs. (12) and (16) together are used for evaluating the energy release rate of the beam. Eq. (12) is used for evaluating the reference coordinate system, r for the applied magnitude of bending moment M. Once the reference coordinate (r) is known, the energy release rate is evaluated by Eq. (16). The analysis is repeated for different magnitudes of bending moment M and the results are summarized in Table 3.

3.2.1 Critical energy release rate (G_c)

In Fig. 1, the reference coordinate r=−0.7 for peak stress. Hence, the critical energy release rate G_c can be evaluated as

$$G_c = L\int_{-1}^{-0.7}\left[\left(473.9e^{0.06458r} - \frac{0.03438}{e^{9.5r}}\right) \times(0.01545r + 0.01546)\,dr\right], \quad (17)$$

then $G_c = 252.02$ kJ/m^2. The results of Table 3 can also be visualized with the help of Fig. 9.

Fig. 9 shows the variation of the energy release rate versus bending moment M acting at the end of the beam. The methodology gives the critical energy release rate as 252.02 kJ/m^2 which corresponds to the magnitude of bending moment M, which initiates yielding in the beam.

Table 3 Energy release rate for a steel beam in pure bending

Bending moment, M (MN·m)	Reference coordinate system, r	Energy release rate (MJ/m^2)	Energy release rate by linear theory (MJ/m^2)
0	−1.0	0	0
0.02695	−0.9	0.01514	0.44375
0.03813	−0.8	0.09409	0.88830
0.04263	−0.7	0.25202	1.11035
0.04548	−0.5	0.80257	1.26377
0.04675	−0.2	2.19679	1.33534
0.04739	0.0	3.50712	1.37195
0.04800	0.2	5.12967	1.40770
0.04894	0.5	8.16585	1.46338
0.04958	0.7	10.60330	1.50190
0.04990	0.8	11.94911	1.52135
0.05055	1.0	14.90010	1.56125

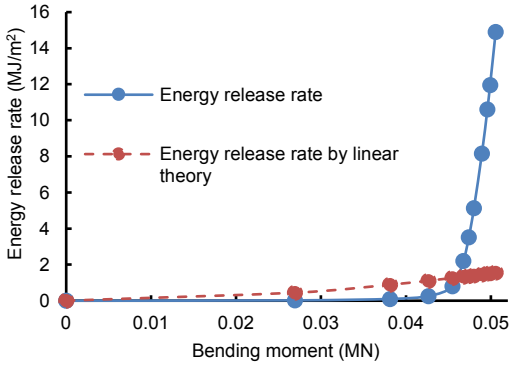

Fig. 9 Variation of Energy release rate with bending moment for the steel beam in pure bending

3.2.2 Energy release rate using linear theory

Using linear theory, the energy release rate of the structure can be evaluated as (Kumar, 2014)

$$G = \frac{d\Pi}{dA} = \frac{d}{dA}(U - W_{ext}), \quad (18)$$

where Π is the total potential of the system, U is internal strain energy stored, and W_{ext} is work done by external loads. Since, in the linear analysis case:

$$\frac{W_{ext}}{dA} = 2\frac{dU}{dA}. \quad (19)$$

For the beam in pure bending in Fig. 8, the strain energy stored U is

$$U = \int \frac{1}{2} Mk\,dL, \quad (20)$$

where k is the curvature of the beam that can be evaluated as

$$k = \frac{M}{EI} = \frac{12M}{Eb(H-h)^3}, \quad (21)$$

where E is the modulus of elasticity of the beam material and I is the moment of inertia of the cross-section. Substituting k into Eq. (20) and integrating, then we can obtain:

$$U = \int \frac{1}{2} M\left(\frac{12M}{Eb(H-h)^3}\right)dL = \frac{6ML}{Eb(H-h)^3}. \quad (22)$$

From Eq. (15), the energy release rate can now be evaluated as

$$G = \frac{dU}{dA} = \frac{d}{bdh}\left[\frac{6ML}{Eb(H-h)^3}\right].$$

After differentiating, we can obtain:

$$G = \frac{18M^2L}{Eb^2(H-h)^3}. \quad (23)$$

3.2.3 Maximum bending moment carrying capacity of the beam

If the failure criteria of the beam are considered as the fracture criteria, i.e. at the point when yielding

starts in the material, the maximum bending moment carrying capacity of the beam can be determined easily by the methodology.

Once the applied bending moment M reaches its maximum value, we consider that the crack starts at the mid length of the beam. If the crack propagates through the depth h, the strain energy stored in the beam will be reduced and can be evaluated by

$$U = bL(H-h)\int_{-1}^{r}\left(473.9\mathrm{e}^{0.06458r} - \frac{0.03438}{\mathrm{e}^{9.5r}}\right) \times (0.01545r + 0.01546)\,\mathrm{d}r. \quad (24)$$

Here, the value of r, i.e. the reference coordinate system, can be taken corresponding to yield stress. It is −0.7 from the stress-strain graph of Fig. 2. For this maximum value of stress at extreme fiber, the magnitude of the couple at the ends can be evaluated by Eq. (12) as

$$473.9\mathrm{e}^{0.06458r} - \frac{0.03438}{\mathrm{e}^{9.5r}} = \frac{4M_x}{b(H-h)^2}. \quad (25)$$

For the increasing depth of crack h, the maximum bending moment carrying capacity of the beam is determined and the results are summarized in Table 4. These results can be visualized in Fig. 10.

As shown in Fig. 10, the maximum moment carrying capacity of the beam decreases as the crack propagates through the depth. This is one of the truly useful outcomes that can be used for evaluating the load-carrying capacity of a structure in the presence of a crack.

Table 4 Maximum bending moment carrying capacity of a steel beam in pure bending

h (mm)	M (MN·m)	h (mm)	M (MN·m)
5	0.04053	60	0.02089
10	0.03848	70	0.01801
20	0.03453	80	0.01534
30	0.03080	90	0.01289
40	0.02728	100	0.01065
50	0.02398		

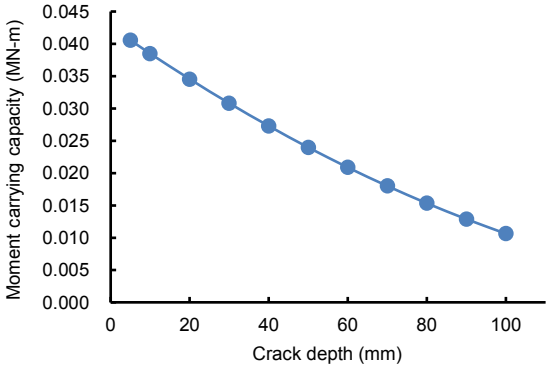

Fig. 10 Maximum bending moment carrying capacity of the steel beam versus crack depth

4 Conclusions

Basic derivation and its numerical validation of deriving shear stress and shear strain functions from normal stress and normal strain functions show the applicability of our methodology for solving 3D problems.

With the solution of a uniaxial bar loaded axially, it can be concluded that this methodology gives realistic results in the plastic range of material behavior and avoids any hypothetical evaluation of stresses and strains, such as those presented by using Green strain and Second Piola-Kirchhoff stress in finite element analysis. The accuracy of the solution by using the Green strain and Second Piola-Kirchhoff stress in finite element analysis is also measured. Using the machine learning regression method, it is observed that even neural networks do not give accurate results in the nonlinear range of the material behavior.

In this paper, we limit the scope to solving the problems for which discretization is not required but the methodology has the scope of further extension for solving problems for which discretization is necessary. The accuracy of the method also depends upon the nonlinear regression method of machine learning used for curve fitting in Python.

The methodology solves a linear, nonlinear or even a fracture problem with relative ease and with simple high-accuracy results in a real physical sense.

Contributors

Himanshu GAUR designed the research. Lema DAKSSA, Mahmoud DAWOOD, and Nitin Kumar SAMAIYA helped in designing and conceptualizing the manuscript.

Conflict of interest

Himanshu GAUR, Lema DAKSSA, Mahmoud DAWOOD, and Nitin Kumar SAMAIYA declare that they have no conflict of interest.

Reference

Amiri F, Millán D, Shen Y, et al., 2014a. Phase-field modeling of fracture in linear thin shells. *Theoretical and Applied Fracture Mechanics*, 69:102-109. https://doi.org/10.1016/j.tafmec.2013.12.002

Amiri F, Anitescu C, Arroyo M, et al., 2014b. XLME interpolants, a seamless bridge between XFEM and enriched meshless methods. *Computational Mechanics*, 53(1):45-57. https://doi.org/10.1007/s00466-013-0891-2

Anitescu C, Atroshchenko E, Alajlan N, et al., 2019. Artificial neural network methods for the solution of second order boundary value problems. *Computers, Materials & Continua*, 59(1):345-359. https://doi.org/10.32604/cmc.2019.06641

Areias P, Rabczuk T, 2013. Finite strain fracture of plates and shells with configurational forces and edge rotations. *International Journal for Numerical Methods in Engineering*, 94(12):1099-1122. https://doi.org/10.1002/nme.4477

Areias P, Rabczuk T, 2017. Steiner-point free edge cutting of tetrahedral meshes with applications in fracture. *Finite Elements in Analysis and Design*, 132:27-41. https://doi.org/10.1016/j.finel.2017.05.001

Areias P, Rabczuk T, Dias-da-Costa D, 2013. Element-wise fracture algorithm based on rotation of edges. *Engineering Fracture Mechanics*, 110:113-137. https://doi.org/10.1016/j.engfracmech.2013.06.006

Areias P, Rabczuk T, Camanho PP, 2014. Finite strain fracture of 2D problems with injected anisotropic softening elements. *Theoretical and Applied Fracture Mechanics*, 72:50-63. https://doi.org/10.1016/j.tafmec.2014.06.006

Areias P, Rabczuk T, Msekh MA, 2016. Phase-field analysis of finite-strain plates and shells including element subdivision. *Computer Methods in Applied Mechanics and Engineering*, 312:322-350. https://doi.org/10.1016/j.cma.2016.01.020

Areias P, Reinoso J, Camanho PP, et al., 2018. Effective 2D and 3D crack propagation with local mesh refinement and the screened Poisson equation. *Engineering Fracture Mechanics*, 189:339-360. https://doi.org/10.1016/j.engfracmech.2017.11.017

Bathe K, 2014. Finite Element Procedures, 2nd Edition. Massachusetts Institute of Technology, Cambridge, USA.

Berg J, Nyström K, 2018. A unified deep artificial neural network approach to partial differential equations in complex geometries. *Neurocomputing*, 317:28-41. https://doi.org/10.1016/j.neucom.2018.06.056

Budarapu PR, Gracie R, Bordas SPA, et al., 2014a. An adaptive multiscale method for quasi-static crack growth. *Computational Mechanics*, 53(6):1129-1148. https://doi.org/10.1007/s00466-013-0952-6

Budarapu PR, Gracie R, Yang SW, et al., 2014b. Efficient coarse graining in multiscale modeling of fracture. *Theoretical and Applied Fracture Mechanics*, 69:126-143. https://doi.org/10.1016/j.tafmec.2013.12.004

Chau-Dinh T, Zi G, Lee PS, et al., 2012. Phantom-node method for shell models with arbitrary cracks. *Computers & Structures*, 92-93:242-256. https://doi.org/10.1016/j.compstruc.2011.10.021

Einstein A, 1916. The foundation of the general theory of relativity. *Annalen der Physik*, 354:769-822. https://doi.org/10.1002/andp.19163540702.

ES6, 2018. Mini Tensile Test Specimens. TecQuipment Ltd., Long Eaton, Nottingham, UK.

Evans PH, Marathe MS, 1968. Microcracking and stress-strain curves for concrete in tension. *Matériaux et Construction*, 1:61-64. https://doi.org/10.1007/BF02479001

Gaur H, 2019. A new stress based approach for nonlinear finite element analysis. *Journal of Applied and Computational Mechanics*, 5:563-576. https://doi.org/10.22055/JACM.2019.29045.1548

Gaur H, Srivastav A, 2020. A novel formulation of material nonlinear analysis in structural mechanics. *Defence Technology*, 17(1):36-49. https://doi.org/10.1016/j.dt.2020.06.018

Gauss CF, 1867. Werke. Cambridge Library Collection–Mathematics. Cambridge University Press, Cambridge, UK.

Ghorashi SS, Valizadeh N, Mohammadi S, et al., 2015. T-spline based XIGA for fracture analysis of orthotropic media. *Computers & Structures*, 147:138-146. https://doi.org/10.1016/j.compstruc.2014.09.017

Griffith AA, 1921. VI. The phenomena of rupture and flow in solids. *Philosophical Transactions of the Royal Society of London Series A*, 221(582-593):163-198. https://doi.org/10.1098/rsta.1921.0006

Guo HW, Zhuang XY, Rabczuk T, 2019. A deep collocation method for the bending analysis of Kirchhoff plate. *Computers, Materials & Continua*, 59(2):433-456. https://doi.org/10.32604/cmc.2019.06660

Hillerborg A, Modéer M, Petersson PE, 1976. Analysis of crack formation and crack growth in concrete by means of fracture mechanics and finite elements. *Cement and Concrete Research*, 6(6):773-781. https://doi.org/10.1016/0008-8846(76)90007-7

Kumar P, 2014. Elements of Fracture Mechanics. Tata McGraw-Hill Education, New Delhi, India.

Lagaris IE, Likas A, Fotiadis DI, 1998. Artificial neural networks for solving ordinary and partial differential equations. *IEEE Transactions on Neural Networks*, 9(5): 987-1000. https://doi.org/10.1109/72.712178

McCulloch WS, Pitts W, 1990. A logical calculus of the ideas

immanent in nervous activity. *Bulletin of Mathematical Biology*, 52(1-2):99-115. https://doi.org/10.1007/BF02459570

Pedregosa F, Varoquaux G, Gramfort A, et al., 2011. Scikit-learn: machine learning in Python. *The Journal of Machine Learning Research*, 12(85):2825-2830.

Rabczuk T, Belytschko T, 2004. Cracking particles: a simplified meshfree method for arbitrary evolving cracks. *International Journal for Numerical Methods in Engineering*, 61(13):2316-2343. https://doi.org/10.1002/nme.1151

Rabczuk T, Belytschko T, 2007. A three-dimensional large deformation meshfree method for arbitrary evolving cracks. *Computer Methods in Applied Mechanics and Engineering*, 196(29-30):2777-2799. https://doi.org/10.1016/j.cma.2006.06.020

Rabczuk T, Areias PMA, Belytschko T, 2007. A meshfree thin shell method for non-linear dynamic fracture. *International Journal for Numerical Methods in Engineering*, 72(5):524-548. https://doi.org/10.1002/nme.2013

Rabczuk T, Zi G, Bordas S, et al., 2008. A geometrically non-linear three-dimensional cohesive crack method for reinforced concrete structures. *Engineering Fracture Mechanics*, 75(16):4740-4758. https://doi.org/10.1016/j.engfracmech.2008.06.019

Rabczuk T, Zi G, Bordas S, et al., 2010a. A simple and robust three-dimensional cracking-particle method without enrichment. *Computer Methods in Applied Mechanics and Engineering*, 199(37-40):2437-2455. https://doi.org/10.1016/j.cma.2010.03.031

Rabczuk T, Bordas S, Zi G, 2010b. On three-dimensional modelling of crack growth using partition of unity methods. *Computers & Structures*, 88(23-24):1391-1411. https://doi.org/10.1016/j.compstruc.2008.08.010

Rabczuk T, Song JH, Zhuang X, et al., 2019. Extended Finite Element and Meshfree Methods. Elsevier, Amsterdam, the Netherlands. https://doi.org/10.1016/C2017-0-00659-6

Raissi M, Karniadakis EG, 2018. Hidden physics models: machine learning of nonlinear partial differential equations. *Journal of Computational Physics*, 357:125-141. https://doi.org/10.1016/j.jcp.2017.11.039

Samaniego E, Anitescu C, Goswami S, et al., 2020. An energy approach to the solution of partial differential equations in computational mechanics via machine learning: concepts, implementation and applications. *Computer Methods in Applied Mechanics and Engineering*, 362:112790. https://doi.org/10.1016/j.cma.2019.112790

Sirignano J, Spiliopoulos K, 2018. DGM: a deep learning algorithm for solving partial differential equations. *Journal of Computational Physics*, 375:1339-1364. https://doi.org/10.1016/j.jcp.2018.08.029

Talebi H, Silani M, Bordas SPA, et al., 2014. A computational library for multiscale modeling of material failure. *Computational Mechanics*, 53(5):1047-1071. https://doi.org/10.1007/s00466-013-0948-2

Talebi H, Silani M, Rabczuk T, 2015. Concurrent multiscale modeling of three dimensional crack and dislocation propagation. *Advances in Engineering Software*, 80: 82-92. https://doi.org/10.1016/j.advengsoft.2014.09.016

Timoshenko SP, Goodier JN, 1970. Theory of Elasticity. 3rd Edition. Mcgraw Hill, New York, USA.

van Rossum G, Drake FL, 2009. Python 3 Reference Manual. CreateSpace, Scotts Valley, CA, USA.

Vu-Bac N, Duong TX, Lahmer T, et al., 2018. A NURBS-based inverse analysis for reconstruction of nonlinear deformations of thin shell structures. *Computer Methods in Applied Mechanics and Engineering*, 331:427-455. https://doi.org/10.1016/j.cma.2017.09.034

Weinan E, Yu B, 2018. The deep Ritz method: a deep learning-based numerical algorithm for solving variational problems. *Communications in Mathematics and Statistics*, 6:1-12. https://arxiv.org/abs/1710.00211

Zhang YM, Gao ZR, Li YY, et al., 2020. On the crack opening and energy dissipation in a continuum based disconnected crack model. *Finite Elements in Analysis and Design*, 170:103333. https://doi.org/10.1016/j.finel.2019.103333

List of electronic supplementary materials

Data S1 Proposed finite element formulation

Data S2 Derivation of shear stress and shear strain functions from normal stress and normal strain functions